Materials Today Bio 23 (2023) 100804

Contents lists available at ScienceDirect

Materials Today Bio

journal homepage: www.journals.elsevier.com/materials-today-bio

Preparation of Phillygenin-Hyaluronic acid composite milk-derived exosomes and its anti-hepatic fibrosis effect

Lihong Gong [1], Honglin Zhou [1], Yafang Zhang, Cheng Wang, Ke Fu, Cheng Ma, Yunxia Li [*]

State Key Laboratory of Southwestern Chinese Medicine Resources, Key Laboratory of StandardizatAion for Chinese Herbal Medicine, Ministry of Education, School of Pharmacy, Chengdu University of Traditional Chinese Medicine, Chengdu, 611137, China

ARTICLE INFO

Keywords:
Phillygenin
Milk exosomes
Hyaluronic acid
Drug delivery system
Liver fibrosis
Autophagy

ABSTRACT

Liver fibrosis remains a serious problem affecting the health of millions of people worldwide. Hepatic stellate cells (HSCs) are the main effector cells in liver fibrosis and their activation could lead to extracellular matrix deposition, which may aggravate the development of liver fibrosis and inflammation. Previous studies have reported the potential of Phillygenin (PHI) as a hepatoprotective agent to inhibit HSCs activation and fibrosis development. However, the poor water solubility of PHI hinders its clinical application as a potential anti-liver fibrosis therapy. Milk-derived exosomes (mEXO) serve as scalable nanocarriers for delivering chemotherapeutic agents due to their excellent biocompatibility. Here, we developed a PHI-Hyaluronic acid (HA) composite mEXO (PHI-HA-mEXO) drug delivery system, in which DSPE-PEG2000-HA was conjugated to the surface of mEXO to prepare HA-mEXO, and PHI was encapsulated into HA-mEXO to form PHI-HA-mEXO. As a specific receptor for HA, CD44 is frequently over-expressed during liver fibrosis and highly expressed on the surface of activated HSCs (aHSCs). PHI-HA-mEXO can bind to CD44 and enter aHSCs through endocytosis and release PHI. PHI-HA-mEXO drug delivery system can significantly induce aHSCs death without affecting quiescent HSCs (qHSCs) and hepatocytes. Furthermore, we carried out in vitro and in vivo experiments and found that PHI-HA-mEXO could alleviate liver fibrosis through aHSCs-targeted mechanism. In conclusion, the favorable biosafety and superior anti-hepatic fibrosis effects suggest a promising potential of PHI-HA-mEXO in the treatment of hepatic fibrosis. However, detailed pharmokinetics and dose-responsive experiments of PHI-HA-mEXO and the mechanism of mEXO loading drugs are still required before PHI-HA-mEXO can be applied clinically.

1. Introduction

Liver fibrosis is a serious problem affecting the health of people worldwide. Fibrosis is a reversible wound-healing response that repeatedly damages the liver from various acute or chronic stimulation [1,2]. As the main effector cells during liver fibrosis, HSCs are activated by pro-inflammatory cytokines and reactive oxygen species secreted by apoptotic hepatocytes and Kupffer cells, and transformed into myofibroblast-like cells, which refer to aHSCs with proliferation and migration ability [3,4]. The aHSCs produce a large amount of collagen-based extracellular matrix. Liver fibrosis may develop into liver cirrhosis and even cancer without timely intervention [5,6].

Liver fibrosis is a major challenge of global health and is mainly alleviated through anti-inflammatory, anti-oxidative, anti-viral and immunomodulatory treatments [7,8]. However, these treatments have various side effects and cannot be applied for long-term medication. Therefore, it is of great significance to explore safe and effective anti-hepatic fibrosis drugs. Traditional medicine has unique advantages in the treatment of hepatic fibrosis. For example, traditional Chinese medicine can exert liver-protecting effect through anti-inflammatory and antioxidant activities [9]. Among them, PHI has significant anti-hepatic fibrosis ability and shows anti-inflammatory effect by reducing the expression of NF-κB [10]. In addition, PHI also exerts anti-hepatic fibrosis effects by modulating gut microbiota and bile acid metabolism [11,12]. However, the poor water solubility and incomplete oral absorption of PHI limit its oral bioavailability, hindering the clinical development of PHI as a therapeutic agent for liver fibrosis [13]. A substantial number of drug delivery systems have been developed to improve the solubility and oral bioavailability of PHI [14]. Among these methods, the exosomes-based drug delivery system exhibits significant

* Corresponding author. No. 1166, Liu Tai Avenue, Wenjiang District, Chengdu, 611137, China.
E-mail address: lyxtgyxcdutcm@163.com (Y. Li).
[1] These authors have contributed equally to this work.

https://doi.org/10.1016/j.mtbio.2023.100804
Received 24 May 2023; Received in revised form 23 July 2023; Accepted 15 September 2023
Available online 16 September 2023

advantages for the delivery of PHI.

Exosomes are emerging as a potential drug delivery carrier with various advantages such as high biocompatibility, enhanced stability, and limited immunogenicity, which can effectively improve the solubility and bioavailability, and reduce the toxicity of drugs [15,16]. Milk is one of the sources of high-quality protein for people, and contains a large number of exosomes [17]. Milk exosomes have no immune rejection and effect on liver and kidney function in the cross-species application and have a stable structure and sufficient yield, suggesting an ideal source of exosomes [17]. In addition, researchers have now been able to modify mEXO and increase their stability and targeting property. Milk exosomes can be isolated and purified by traditional differential ultracentrifugation and ultrafiltration as well as density gradient centrifugation, polyethylene glycol precipitation, and size exclusion chromatography [18]. Furthermore, mEXO have superior biocompatibility compared to other synthesized nanocarriers, and they are able to alter the pharmacokinetics and in vivo distribution of the loaded drug after oral administration [19].

Previous studies have found that the activation of HSCs plays a crucial role in the development of liver fibrosis [20]. Therefore, targeting the highly expressed receptors on the surface of aHSC is a potential method to improve the drug delivery efficiency and reverse the development of liver fibrosis. HA is a biocompatible, degradable, non-immunogenic, non-toxic, and non-sulfated glycosaminoglycan, which mainly exists in animal extracellular matrix, connective tissue and organs [21]. As a receptor of HA, CD44 is overexpressed during liver injury and plays an important role in aHSCs migration [22]. Therefore, we aim to modify mEXO with HA and develop a CD44 receptor-based targeting delivery system for PHI.

The current research focuses on the development of nanocarrier of HA-modified mEXO encapsulated with PHI (PHI-HA-mEXO) for hepatic fibrosis treatment. We performed comprehensive physicochemical characterization and in vitro stability studies of PHI-HA-mEXO. In addition, we also investigated the biodistribution and anti-fibrotic activity of PHI-HA-mEXO in TGF-β1-induced LX2 cell liver fibrosis and thioacetamide (TAA)-induced liver fibrosis in zebrafish.

2. Materials and methods

Milk from Holstein cows was obtained from a local dairy. PHI (Cat. No. 21080708) was obtained from Chengdu MUST Bio-technology Co., Ltd. (Chengdu, China). DSPE-PEG2000-HA (Cat. No. R-A66001-2 k) was synthesized by Ruisen Beier Bio-technology Co., Ltd. (Shaanxi, China). TGF-β1 (Cat. No. CA59) was obtained from Novoprotein Scientific Inc. (Shanghai, China). LX2 cells were obtained from Central South University (Changsha, China). Human normal liver cells LO2 (iCell-h054) were purchased from iCell Bioscience (Shanghai, China). Human umbilical vein endothelial cells (HUVECs) and human lung epithelial cells (A549) were obtained from Chengdu University of Traditional Chinese Medicine (Sichuan, China). Tricaine was purchased from Sigma-Aldrich (Shanghai, China). BCA Protein Assay kit (Cat. No. G2026-1000T) was collected from MultiSciences Biotech Co., Ltd (Hangzhou, China). Rabbit anti-human HA (Cat. No. CPA182Ge21; Dilution 1:1000), rabbit anti-human CD9 (Cat. No. YT0782; Dilution 1:1000), rabbit anti-human CD81 (Cat. No. YT5394; Dilution 1:1000), and rabbit anti-human Calnexin (Cat. No. YT0613; Dilution 1:1000) were collected from Cloud-clone Corp. (Wuhan, China) and Immunoway Bio-technology (USA). Rabbit anti-α-SMA (Cat. No. AF1031; Dilution 1:200), rabbit anti-Col1α1 (Cat. No. AF7001; Dilution 1:200), and rabbit anti-Lamin B1 (Cat. No. AF5161; Dilution 1:400) were purchased from Affinity Biosciences. Goat anti-rabbit IgG-HRP (Cat. No. 05-4030-05; Dilution 1:5000) were obtained from Multi Sciences Biotech Co., Ltd. (Hangzhou, China). Methanol of HPLC (Cat. No. 216565) grade were collected from Merck Chemicals (Shanghai, China). RPMI Medium 1640 basic (1 ×) (Cat. No. 8122651) and DMEM basic (1 ×) (Cat. No. 8122340) were obtained from gibco (Australia). CD44 (Cat. No. AF6186) was collected from Affinity Biosciences (Jiangsu, China). Annexin-V-FITC Apoptosis Detection Kit (Cat. No. E-CK-A211) was collected from Elabscience biotechnology Co., Ltd. (Wuhan, China). DIR (Cat. No. D4006) was purchased from UElandy Inc. (Suzhou, China). 4% paraformaldehyde (Cat. No. G1101) was purchased from Servicebio Technology Co., Ltd. (Wuhan, China). Total RNA Isolation kit (Cat. No. RE-03014) was obtained from FOREGENE Biotechnology Co. Ltd. (Chengdu, China). ABScript III RT Master Mix for qPCR (Cat. No. 20428) and Genious 2× SYBR Green Fast qPCR Mix (No ROX) (Cat. No. 21205) were obtained from ABclonal Technology Co., Ltd. (Wuhan, China). PCR primer sequences were synthesized in TSINGKE Biological Technology (Chengdu, China).

2.1. Isolation and purification of mEXO

Differential ultracentrifugation is currently the most commonly used method to isolate and purify exosomes and remains the gold standard for exosomes isolation to date, although other techniques such as density gradient centrifugation, polyethylene glycol precipitation, and size exclusion chromatography approaches are common [23–26]. In this study, exosomes were extracted from milk using differential ultracentrifuga-tion, which can obtain exosomes with uniform size by adopting low-speed and high-speed centrifugation in sequence [27,28]. Briefly, milk was put into several 50 mL centrifuge tubes, and centrifuged at 10,000×*g* for 30 min (Avanti X–30R, Beckman Coulter Inc.) to remove fat globules, casein aggregates, cell debris, and collect skim milk. The skimmed milk was then transferred to several 38.4 mL ultracentrifuge tubes and centrifuged using an Optima XPN-100 Ultracentrifuge (Beckman Coulter Inc.) (100,000×*g*, 90 min, 4 °C). The upper whey was collected and centrifuged using an ultracentrifuge for 70 min (135,000×*g*, 4 °C), and the supernatant was discarded to harvest the mEXO pellet. The mEXO was then washed three times with pre-cooled PBS solution, and resuspended into PBS.

2.2. Preparation of PHI-HA-mEXO and encapsulation efficiency assay

To prepare PHI-HA-mEXO, mEXO were first decorated with DSPE-PEG2000-HA (20:1, weight ratio) by incubating for 48 h at 37 °C, followed by centrifugation to remove unbound ligands and obtain HA-mEXO (3500×*g*, 10 min) [29]. According to Wu's study, functional modification of exosomes enabled the spontaneous decoration of HA conjugate onto the mEXO phospholipid bilayer [29]. Specifically, HA-activated ester was connected with lipophilic DSPE-PEG2000-NH2 to form DSPE-PEG2000-HA conjugate. The lipophilic DSPE can be inserted into the phospholipid bilayer of exosomes by self-assembly. The flexible connecting arm of polyethylene glycol PEG2000 has good biocompatibility and contributes to the successful exposure of HA on the exosome surface to form HA-mEXO [29]. Subsequently, HA-mEXO and PHI were loaded at a mass ratio of 6:1 and incubated at room temperature for 3 h in the dark. The unbound PHI was removed by ultrafiltration with a 10 KDa ultrafiltration tube at 3500×*g* for 10 min to obtain the purified PHI-HA-mEXO.

To evaluate the encapsulation capacity of mEXO on PHI, the drug loading efficiency of PHI was determined by high performance liquid chromatography (HPLC, Agilent 1260 Infinity). The preparation of reference solution was as follows: precisely weigh a certain amount of PHI into a 5 mL volumetric flask, add methanol to the volume, and obtain the mother liquor. The preparation of the test solution was as follows: take 10 μL of the PHI-HA-mEXO suspension, add 790 μL of methanol to break the emulsion. Chromatographic column equipped with Agilent ZORBAX Eclipse Plus C18 (4.6 × 250 mm, 5 μm) was performed in this study. The detection wavelength was set at 280 nm. The column temperature was set at 25 °C. The injection volume was 10 μL. A linear gradient of methanol and water was set as shown in Table 1. The peak area of the obtained sample was detected by HPLC instrument, and the concentration and encapsulation efficiency were calculated

Table 1
HPLC gradient elution procedure.

Time (min)	Methanol (%)	Water (%)
0	50	50
10	50	50
20	40	60
30	20	80

Characterization of mEXO and PHI-HA-mEXO.

according to the standard curve. The calculation formula of the encapsulation efficiency was as follows: encapsulation efficiency = (the amount of PHI in PHI-HA-mEXO/the total amount of PHI added) × 100%.

10 μL of mEXO and PHI-HA-mEXO were dropped on the copper mesh for 1 min, the remaining liquid was carefully absorbed with filter paper, followed by the addition of 10 μL 1% uranyl acetate added for negative staining for 5 min. Subsequently, the excess negative staining solution on the filter paper was absorbed and dried for 30 min at room temperature. The morphology of mEXO and PHI-HA-mEXO was observed and imaged using a scanning electron microscopy (SEM) (Hitachi, HT-7700) under 100 kV.

The nanoparticle tracking analyzer (Particle metrix, Zetaview, Germany) was performed to detect and record the size distribution, zeta potential, and concentration (number of vesicles/mL) of exosomes (Measurement Parameters: Cell S/N: ZNTA; Analysis Parameters: Max Area: 1000, Min Area: 5, Min Brightness: 20). Specifically, the extracted mEXO and PHI-HA-mEXO were diluted to 1000-fold with deionized water, and 1 mL of the homogenous sample was injected into the analyzer.

To detect the membrane proteins of exosomes, mEXO or PHI-HA-mEXO was mixed with protein loading buffer at a ratio of 4:1, and treated at 100 °C for 10 min for protein denaturation. 10 μL of the protein sample was loaded for electrophoresis, and then transferred to a PVDF membrane. The membrane was treated with HA, CD9, CD81 and Calnexin primary antibodies (Dilution 1:1000) overnight. After incubation, the PVDF membrane was washed three times with TBST solution and incubated with the secondary antibody (IgG-HRP; Dilution 1:5000) for 2 h. After incubation, the PVDF membrane was washed three times with TBST solution and imaged following the instructions of the ultrasensitive ECL chemiluminescence kit.

2.3. Storage stability study

Since the constructed drug loading system is mainly based on exosomes, the biofilm material is not suitable for long-term storage at 4 °C. In order to explore the storage conditions of the drug-loading system to perform the subsequent experiments, the PHI-HA-mEXO system was stored in a −80 °C refrigerator. The exosomes particles were detected by a nanoparticle tracking analyzer after one month storage. The morphology, diameter, and zeta potential changes of PHI-HA-mEXO were detected to evaluate the stability.

2.4. Uptake of mEXO

To assess the uptake of exosomes, we first labeled PHI-HA-mEXO and PHI-mEXO with fluorescent dye DIR at a final concentration of 10 μM for 30 min at 37 °C. The free fluorescent dye was removed by using an ultrafiltration tube (10 min, 3500×*g*, 4 °C) to obtain the labeled exosomes. LX2 cells were seeded in confocal dishes (1×10^6 cells/dish) and incubated overnight. To study the intracellular uptake of PHI-HA-mEXO, we first constructed a cell liver fibrosis model with 15 ng/mL TGF-β1. Subsequently, we investigated the intracellular uptake of PHI-HA-mEXO and PHI-mEXO in normal and TGF-β1-stimulated LX2 cells. Specifically, LX2 cells were incubated without TGF-β1 or with TGF-β1 and DIR-labeled PHI-HA-mEXO or PHI-mEXO for 4 h. After incubation, LX2 cells were washed with PBS and fixed with 4% paraformaldehyde and stained by DAPI. The uptake of PHI-HA-mEXO or PHI-mEXO was observed under the laser confocal microscope (Leica TSC SP8, Germany).

2.5. Cell culture, cell viability and cytotoxicity

LO2 cells were cultured in DMEM medium supplemented with 10% FBS and 1% antibiotics. LX2, HUVECs, and A549 cells were cultured in 1640 medium supplemented with 10% fetal bovine serum (FBS) and 1% antibiotics. Cells at about 80% confluence were seeded into 96-well plates (5×10^3 cells/well) and incubated overnight. Subsequently, LX2, LO2, HUVECs, and A549 cells were treated with different concentrations of PHI-HA-mEXO (3.75, 7.5, 15, 30, 60, and 120 μg/mL) for 24 h. The medicated medium was then discarded and 20 μL of MTT solution was added and incubated for 4 h. Finally, the absorbance at 490 nm was measured using a microplate reader (Thermo Scientific, USA).

2.6. CD44 expression assay

LX2 cells were seeded on confocal dishes (1×10^6 cells/dish) and divided into control group, model group, PHI-mEXO group and PHI-HA-mEXO group. In the control group, LX2 cells were cultured without TGF-β1 or drugs for 24 h. In the model group, LX2 cells were treated with 15 ng/mL TGF-β1 for 24 h. In PHI-mEXO group and PHI-HA-mEXO group, LX2 cells were treated with 15 ng/mL TGF-β1 and/or 30 μg/mL PHI-HA-mEXO and 30 μg/mL PHI-mEXO for 24 h. After treatment, LX2 cells were fixed with 4% paraformaldehyde at room temperature and blocked with normal non-immune serum (goat). Subsequently, LX2 cells were incubated with primary antibody CD44 (1:375) at 4 °C overnight, followed by goat anti-rabbit red fluorescent secondary antibody (1:2000) incubation at room temperature for 30 min. The nuclei were stained and mounted with DAPI reagent. The cells were then observed and photographed using a confocal microscope.

LX2 cells were seeded on six-well plates (1×10^6 cells/well) and grouped and administrated as mentioned above. After treatment, the cells were washed with PBS, and the CD44 antibody was added for 30 min incubation in the dark for flow cytometry analysis, and the expression levels of CD44 in each group were calculated.

2.7. Immunofluorescence staining

LX2 cells were cultured on confocal dishes (1×10^6 cells/dish) and divided into control group, model group, and PHI-HA-mEXO (7.5, 15, 30 μg/mL) groups. In the control group, LX2 cells were cultured without TGF-β1 or drugs for 24 h. In the model group, LX2 cells were treated with 15 ng/mL TGF-β1 for 24 h. In PHI-HA-mEXO groups, LX2 cells were treated with 15 ng/mL TGF-β1 and different concentrations of PHI-HA-mEXO (7.5, 15, 30 μg/mL) for 24 h. After treatment, LX2 cells were fixed with 4% paraformaldehyde at room temperature and blocked with normal non-immune serum (goat). LX2 cells were then incubated with α-SMA or Col1α1 antibodies (1:200) at 4 °C overnight. The next day, the cells were treated with goat anti-rabbit red fluorescent secondary antibody (1:400) at room temperature for 30 min and counterstained with DAPI. The images were obtained using a confocal microscope.

2.8. Apoptosis assay

LX2 cells were seeded on six-well plates (1×10^6 cells/well) and treated with TGF-β1 in the presence or absence of PHI-HA-mEXO (7.5, 15, 30 μg/mL) for 24 h. After administration, cells were trypsin digested and suspended in the binding buffer. Subsequently, LX2 cells were stained with Annexin V-FITC and PE and treated for 15 min, followed by flow cytometry analysis.

2.9. In vivo biodistribution study of PHI-HA-mEXO

Liver fibrotic zebrafish larvae and normal zebrafish larvae were treated with DIR dye-labeled PHI-HA-mEXO or PHI-mEXO (100 μM) for 3 days. The solution was changed every 24 h. After treatments, the larval zebrafish were anesthetized and placed on a confocal dish, and the fluorescence was observed using a confocal microscope at excitation and emission wavelengths of 750 and 779 nm.

2.10. Animal study

A TAA-induced liver fibrosis model was constructed using two days post fertilization (dpf) liver-specific transgenic zebrafish (fabp10a: EGFP), in which liver fatty acid binding protein was labeled with an enhanced green fluorescent protein. All procedures were approved by the Animal Experiment Ethics Committee of Chengdu University of Traditional Chinese Medicine. In this experiment, drugs were added to the embryonic medium for oral administration [30,31]. Zebrafish larvae at 2 dpf were randomly divided into 12-well plates (15 larvae/well) and incubated with 2 mL embryonic medium or drugs. The larvae were grouped as follows: control group (embryonic medium), 10 mM TAA control group, PHI-HA-mEXO groups (10 mM TAA and 25, 50, 100 μM PHI-HA-mEXO), HA-mEXO group (10 mM TAA and 100 μM HA-mEXO), PHI-mEXO group (10 mM TAA and 100 μM PHI-mEXO), PHI group (10 mM TAA and 100 μM PHI), and mEXO group (10 mM TAA and 100 μM mEXO). All agents were dissolved in the embryonic medium and the solution was changed every 24 h. The amounts of HA-mEXO, PHI--mEXO, PHI and mEXO were fixed to equal amounts of 100 μM PHI-HA-mEXO. After drug administration, the larvae were photographed using a fluorescence microscope (Nikon, Ts2), and the liver area and fluorescence intensity were quantified by image pro plus software.

2.11. Biochemical analysis and histopathological examination of liver tissue

Zebrafish larvae from the control, model, and PHI-HA-mEXO (25, 50, 100 μM) groups were administrated as described above. After treatments, liver tissue samples were fixed with 4% paraformaldehyde for 24 h, dehydrated in ethanol, embedded and sectioned at 5 μm. The paraffin sections were successively dewaxed, rehydrated, stained with hematoxylin, differentiated, and stained with eosin. HE staining and Sirius red staining were performed, and histopathological examination was carried out under a microscope.

2.12. Real-time quantitative PCR (RT-qPCR) analysis

Total RNA was extracted from LX2 cells or larval zebrafish using a total RNA isolation kit dissolved in 50 μL of RNase-free water according to the manufacturer's instructions. The purity of RNA was characterized by the OD260/280 value measured by a nucleic acid/protein analyzer. HiScript® III All-in-one RT SuperMix Perfect for qPCR performs reverse transcription to synthesize cDNA. The reaction conditions were set as follows: 25 °C for 5 min, 42 °C for 15 min and 85 °C for 5 s. RT-qPCR was performed on the StepOnePlus Real-Time PCR System by adding 2 × Taq Pro Universal SYBR qPCR Master Mix according to the manufacturer's protocol. The reaction conditions were set as follows: 95 °C for 1 min, followed by 40 cycles of 5 s at 95 °C and 30 s at 60 °C. The specific sequences of primers used in this study were synthesized by TSINGKE Biological Technology (Chengdu, China) and primers sequences were listed in Table 2. The $2^{-\triangle\triangle Ct}$ method was used to calculate the relative expression level of the target genes.

2.13. Statistical analysis

Statistical analysis was performed using SPSS 26.0 software (Chicago, IL, USA). The results were expressed as mean ± standard deviation, and one-way analysis of variance (One-Way ANOVA) was used for statistical analysis. $P < 0.05$ was considered statistically significant.

3. Results

3.1. Physical and chemical characterization of mEXO and PHI-HA-mEXO

The results of transmission electron microscopy showed that exosomes extracted by differential centrifugation had good dispersion, and exhibited circular or quasi-circular saucer-like/cup-like structures, with obvious membrane-like structures and borders. The clear and concentrated distribution suggested that the obtained exosomes have preferable size uniformity (Fig. 1A).

The results of nanoparticle tracking analysis showed that the membrane surface was negatively charged, and the zeta potential of mEXO and PHI-HA-mEXO were −36.41 ± 1.63 mV and −36.77 ± 1.21 mV respectively (Fig. 1B). The particle size of mEXO ranged from 80 to 140 nm, with an average size of 114.2 nm (Fig. 1C), and the concentration was 6.0×10^{10} Particles/mL. The particle size of PHI-HA-mEXO ranged from 80 to 130 nm, with an average particle size of 120.7 nm (Fig. 1C), and the concentration was 2.7×10^{11} Particles/mL.

Western blot results showed that the obtained mEXO and PHI-HA-mEXO expressed the characteristic membrane proteins CD9 and CD81, but not the negative protein Calnexin (Fig. 1D). In addition, HA was identified in PHI-HA-mEXO, but not in mEXO, indicating that HA was successfully integrated into exosomes.

3.2. Drug loading efficiency, stability and in vitro release assay

According to the injection concentration and peak area of the PHI standard, the linear regression equation of the standard curve is calculated as $Y = 42.457X\text{-}70.798$ ($R^2 = 0.9997$), and PHI has a good linear relationship in the mass concentration range of 3.125–700 mg/L. Fig. 2A

Table 2
Specific primers sequences used in RT-qPCR.

Gene	Sense primer (5′ to 3′)	Antisense primer (5′ to 3′)
Cell model		
α-SMA	ACTGCCTTGGTGTGTGACAA	CACCATCACCCCCTGATGTC
Collagen-1	CCTGGATGCCATCAAAGTCT	CGCCATACTCGAACTGGAAT
GAPDH	ACTAGGCGCTCACTGTTCT	CCAATACGACCAAATCCGTTG
Zebrafish model		
α-SMA	TGATGAAGCCGGACCCTCTA	AGAAGTGGGCAGTGCAAAGA
Collagen-1	ACCGAACATGCGAGCACTAC	TGTGGTTCCAGTCACGACAC
LC3	ACATCATGGATGGGCTACGG	GTGCCGCTCACGATGATTTT
Beclin1	ACTATCCACGAGCTCACTGC	AATTTTCGAGCCACGCCATC
P62	ATCTGCGCCATCAGCCTTTG	GAGCGGAGAATTCAAGCAGC
Atg5	CGTTTGGATGCAGTAGTGTTTGTA	AAACAGGCGGGTATCCTTCC
Atg7	TGGAGGATCTGACCGGCTTA	GCTCTCGTCGTCACTCATGT
GAPDH	GGATCTGACAGTCCGTCTTGAGAA	CCATTGAAGTCAGTGGACACAACC

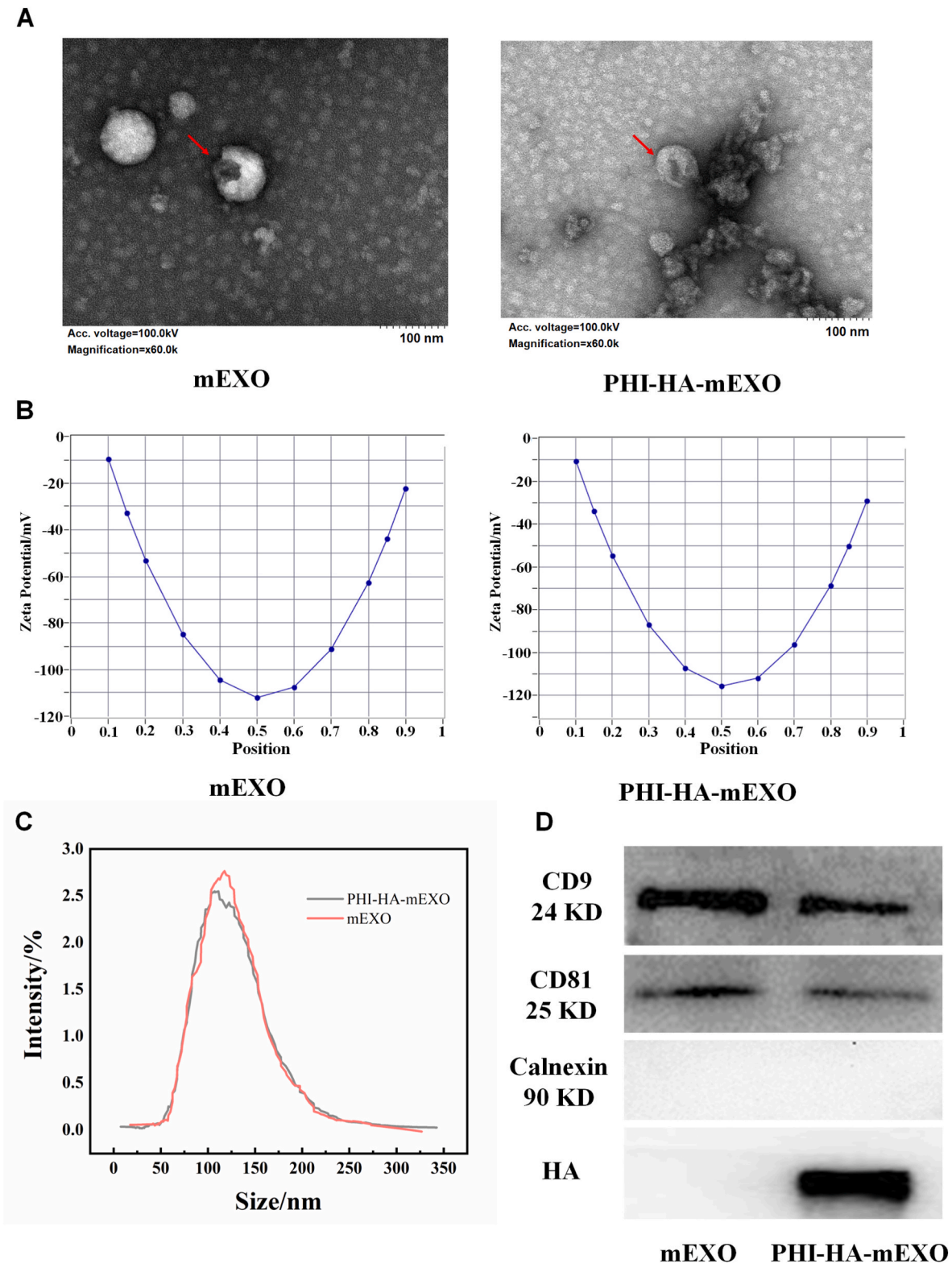

Fig. 1. Physicochemical properties of mEXO and PHI-HA-mEXO. (A) Representative transmission electron microscopy images of mEXO and PHI-HA-mEXO. (B) Representative photograph of zeta potential of mEXO and PHI-HA-mEXO. (C) The particle size distribution of mEXO and PHI-HA-mEXO. (D) Western blot assay of CD9, CD81, Calnexin proteins and HA polysaccharide in mEXO and PHI-HA-mEXO.

showed the representative chromatograms of PHI and emulsified PHI-HA-mEXO. The drug loading efficiency of PHI was calculated by the regression equation of the PHI standard curve. As a result, the loading efficiency of PHI on mEXO was measured to be 57.06%, which was beneficial to perform subsequent pharmacological experiments.

The particle size and potential changes of PHI-HA-mEXO after being stored in a −80 °C refrigerator for one month were measured by a nanoparticle tracking analyzer. As shown in Fig. 2B, the particle size of PHI-HA-mEXO was 120.5 nm, and the zeta potential was −33.21 ± 0.00 mV, and exhibited a saucer-like structure. Therefore, compared with

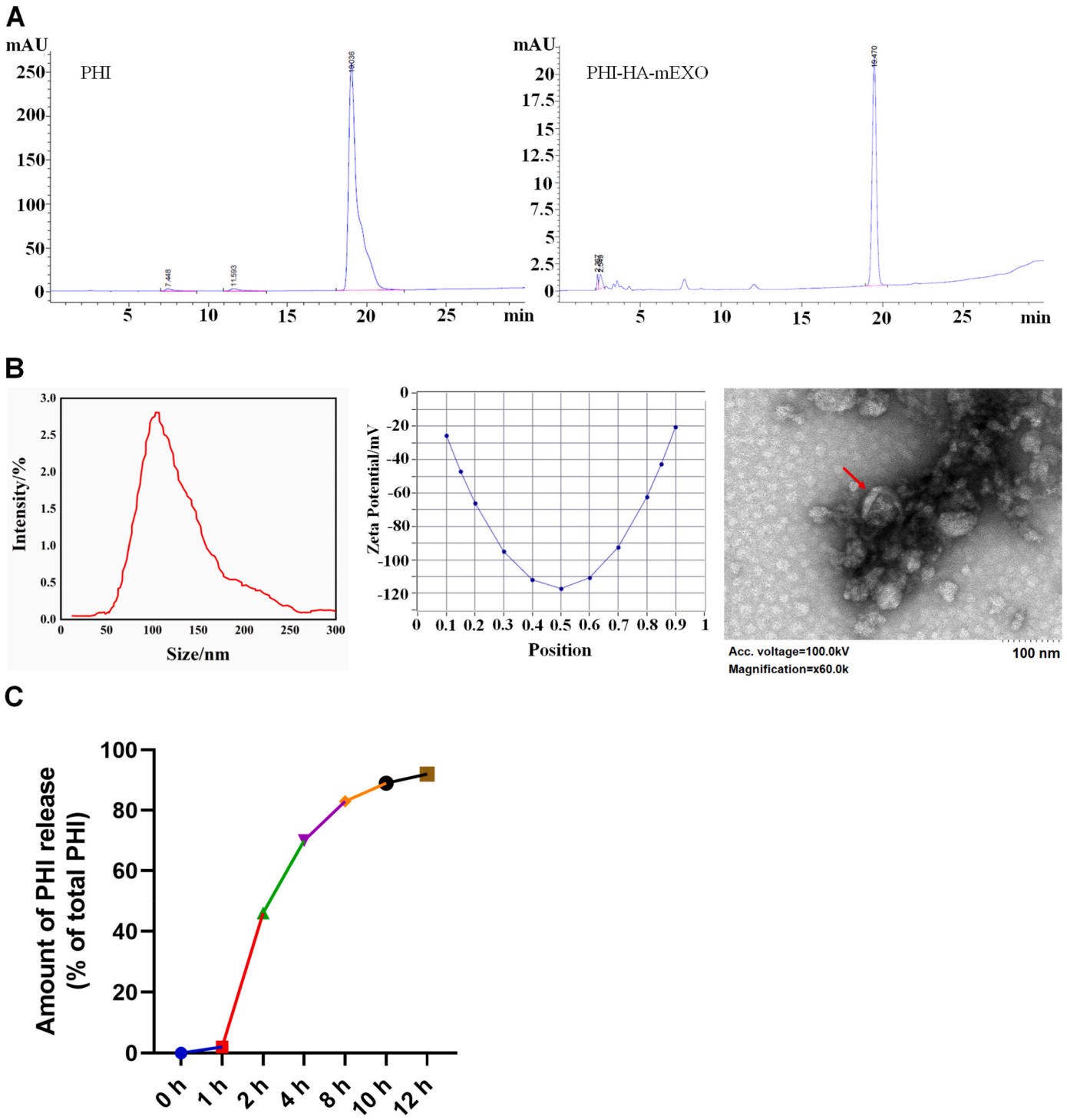

Fig. 2. Drug loading efficiency, stability and in vitro release assay of PHI-HA-mEXO. (A) The representative HPLC chromatograms of PHI and emulsified PHI-HA-mEXO. (B) The particle size, zeta potential, and morphology of PHI-HA-mEXO after cryogenic storage for one month. (C) The release profile of PHI-HA-mEXO in PBS at pH 7.4.

freshly prepared samples, the nanoparticle properties did not change significantly after one month storage. These findings suggest that PHI-HA-mEXO can be stored at −80 °C without causing significant changes in physicochemical properties.

The drug release kinetics of PHI-HA-mEXO were determined using a dialysis bag in PBS buffer solution. The results showed that PHI-HA-mEXO exhibited time-dependent release. After 1, 2, 4, and 8 h, the cumulative release of PHI was 2%, 46%, 70%, and 83%, respectively, and almost all drugs (92%) were released after 12 h (Fig. 2C).

3.3. Uptake of PHI-HA-mEXO and CD44 assessment

Studies have shown that milk exosomes are protected by a phospholipid bilayer, the barrier prevents the cargo in exosomes from degrading in the gastrointestinal tract and being absorbed deeper in the gut, and have an enhanced intestinal permeability [32,33]. Therefore, the substances encapsulated in milk exosomes could resist harsh digestion processes and reach the small intestine, where they are absorbed and transferred into the bloodstream [34,35]. The uptake of

PHI-HA-mEXO in normal and TGF-β1 stimulated LX2 cells was observed using a laser confocal microscope, and the uptake of PHI-mEXO served as a control. As shown in Fig. 3A, the uptake of PHI-HA-mEXO and PHI-mEXO showed no significant difference in qHSCs (without TGF-β1 stimulation). However, the uptake of PHI-HA-mEXO was significantly increased in aHSCs and higher than that of PHI-mEXO. In addition, we observed the uptake of DIR-labeled PHI-HA-mEXO and PHI-mEXO in normal and TAA-induced liver fibrosis in zebrafish larvae (Fig. 3B). As a

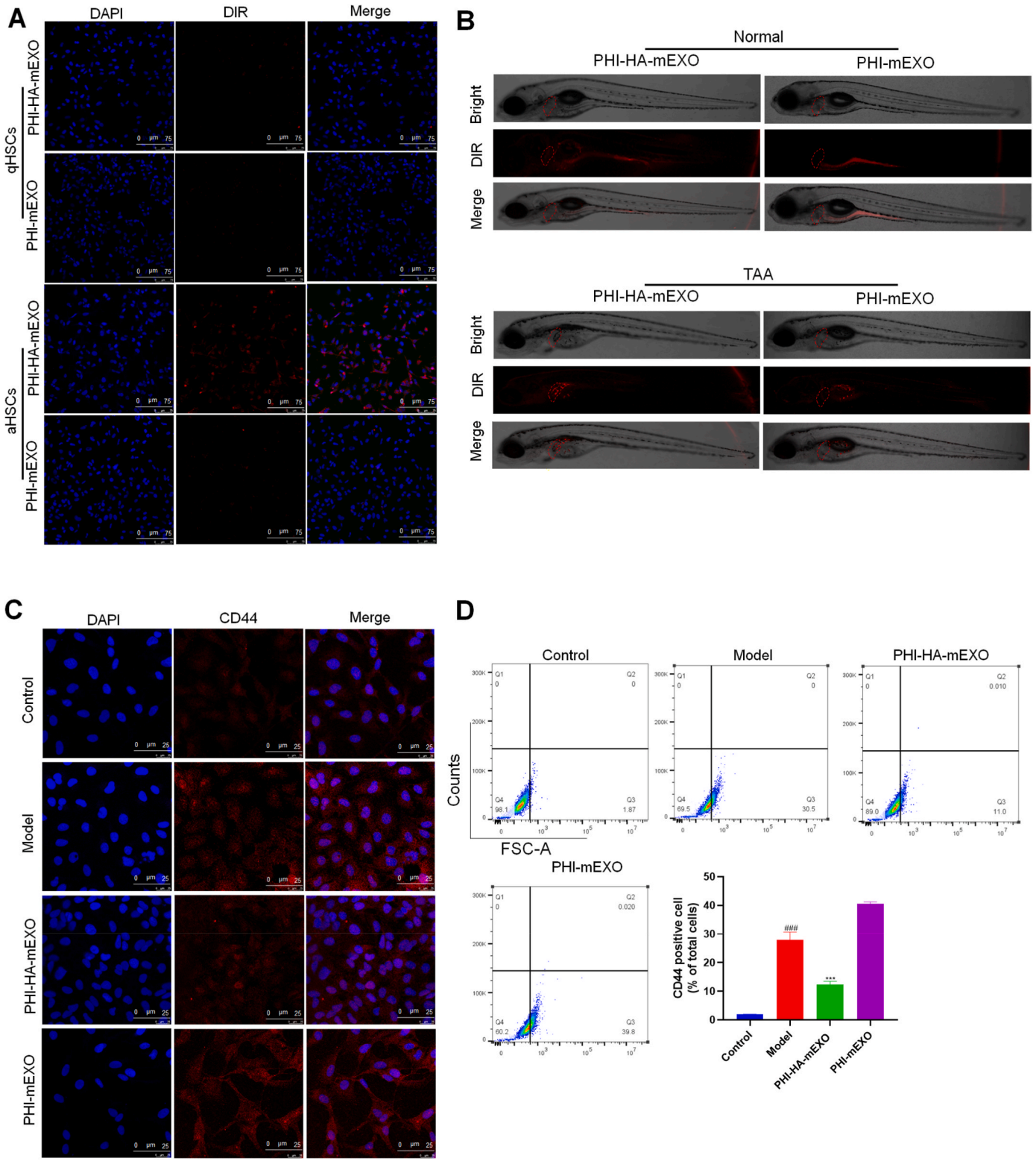

Fig. 3. Uptake of PHI-HA-mEXO and CD44 assessment. (A) The uptake of DIR-labeled PHI-HA-mEXO and PHI-mEXO in qHSCs and aHSCs. (B) The uptake of DIR-labeled PHI-HA-mEXO and PHI-mEXO in normal and TAA-induced liver fibrosis in zebrafish larvae. (C) Representative confocal images of CD44 signals in normal and TGF-β1-activated LX2 cells. (D) Representative images of the flow cytometry results of CD44 signals in normal and TGF-β1-activated LX2 cells. Data were shown as mean ± SD (n = 3). $^{###}p < 0.001$ compared with the control group; $^{***}p < 0.001$ compared with the model group.

result, PHI-HA-mEXO and PHI-mEXO did not significantly aggregate in the zebrafish liver in the normal control group. However, PHI-HA-mEXO showed an increased accumulation in the liver area after TAA exposure, and PHI-mEXO did not show this effect. These findings indicated that HA modification could improve the uptake of drug-loaded exosomes and suggested a high-efficiency targeting ability of PHI-HA-mEXO to CD44 overexpressed cells and tissues.

CD44 is overexpressed in aHSCs and almost not expressed in qHSCs. As a unique ligand of CD44, HA can specifically bind to CD44 and downregulate its expression [36]. To assess this effect of PHI-HA-mEXO, we detected the expression of CD44 in aHSCs and qHSCs by immunofluorescence and flow cytometry. As shown in Fig. 3C, there were very few CD44 signal in the control group. However, high levels of CD44 expression were observed in LX2 cells after TGF-β1 stimulation. In addition, the expression level of CD44 in the PHI-HA-mEXO group was lower than those in the model group and PHI-mEXO group. Moreover, we measured the CD44 positive cells using flow cytometry and the results were shown in Fig. 3D. The ratio of CD44 positive cells was increased in the model group compared with the control group. However, PHI-HA-mEXO treatment significantly down-regulated the CD44 expression compared with the model group and PHI-mEXO group, indicating that PHI-HA-mEXO could bind to CD44 and block the accessibility of antibodies to CD44. These results indicated that PHI-HA-mEXO could interact with CD44 in aHSCs.

3.4. Anti-hepatic fibrosis effect of PHI-HA-mEXO

First, we constructed a liver fibrosis cell model and evaluated the anti-fibrotic properties of PHI-HA-mEXO (3.75, 7.5, 15, 30, 60 and 120 μg/mL) using TGF-β1-treated LX2 cells. The results were shown in Fig. 4A, compared with the control group, TGF-β1 significantly promoted the proliferation of LX2 cells, indicating that the liver fibrosis model was successfully established. However, compared with the model group, the viability of LX2 cells decreased with the increase of the concentration of PHI-HA-mEXO and reversed to normal level at 30 μg/mL. Therefore, we chose 7.5, 15, 30 μg/mL concentrations for further study.

In order to verify whether the drug loading system has superior anti-hepatic fibrosis effect, we explored the anti-hepatic fibrosis effect of PHI-HA-mEXO, PHI-mEXO, HA-mEXO, PHI, mEXO at the administration concentration of 30 μg/mL. The results were shown in Fig. 4B, the cell viability in mEXO group, HA-mEXO group, PHI group and PHI-mEXO group showed no differences compared with the model group, while the PHI-HA-mEXO group exhibited significant anti-hepatic fibrosis properties.

Subsequently, we have carried out RT-qPCR experiments to evaluate the effect of PHI-HA-mEXO on the expression of fibrosis cytokines α-SMA and Col1α1. As shown in Fig. 4C, RT-qPCR results indicated that PHI-HA-mEXO could significantly inhibit the expression levels of α-SMA and Col1α1 in LX2 cells, while mEXO group, HA-mEXO group, PHI group and PHI-mEXO group could not inhibit the expression levels of α-SMA and Col1α1. In addition, we carried out immunofluorescence to evaluate the effect of PHI-HA-mEXO on α-SMA and Col1α1 expression. As shown in Fig. 4D and E, compared with control group, TGF-β1 exposure significantly increased α-SMA and Col1α1 expression. However, PHI-HA-mEXO could inhibited the immunofluorescence intensity of α-SMA and Col1α1 induced by TGF-β1, suggesting that PHI-HA-mEXO could reverse the *trans*-differentiation of fibroblasts to myofibroblasts to mitigate hypertrophic scar fibrosis.

According to reports, apoptotic aHSCs have been observed during the development of liver fibrosis, and rapid apoptosis of aHSCs has been confirmed to play an important role in the regression of fibrosis [37,38]. Therefore, we have detected the effect of PHI-HA-mEXO on aHSCs apoptosis. Flow cytometry results showed that PHI-HA-mEXO could promote LX2 cell apoptosis (Fig. 4F), suggesting that PHI-HA-mEXO could alleviate liver fibrosis via inducing apoptosis of aHSCs.

3.5. Safety evaluation of PHI-HA-mEXO

To evaluate the biosafety of PHI-HA-mEXO, we investigated the cytotoxicity of PHI-HA-mEXO on normal hepatocytes L02 cells ($CD44^-$), LX2 cells ($CD44^-$), endothelial cells HUVECs ($CD44^+$), and epithelial cells A549 ($CD44^+$). After different concentrations of PHI-HA-mEXO (3.75, 7.5, 15, 30, 60, 120 μg/mL) treatment for 24 h, the cell viability of LO2, LX2, HUVECs, and A549 cells were not affected at concentrations less than 30 μg/mL (Fig. 5). However, 120 μg/mL PHI-HA-mEXO substantially inhibited the viability of LO2, LX2, and HUVECs cells, demonstrating that PHI-HA-mEXO had no effect on cells viability when the dose was less than 30 μg/mL, but showed an inhibitory effect at a high concentration. The results indicated that PHI-HA-mEXO is safe for the treatment of liver fibrosis and has good biocompatibility.

3.6. Anti-liver fibrosis effect of PHI-HA-mEXO in zebrafish model

Two dpf zebrafish larvae were soaked in TAA for three days to establish liver fibrosis model. In this study, we used liver-specific transgenic zebrafish (fabp10a: EGFP), in which liver fatty acid binding protein was labeled with an enhanced green fluorescent protein. Therefore, the fluorescent intensity and area represent the liver function of zebrafish. As reported, TAA-induced liver fibrosis could lead to the decrease of liver volume and weakened fluorescent intensity [31,39]. As shown in Fig. 6A and Fig. S1, the larvae displayed a clear and strong fluorescence signal in the normal control group. However, the larvae treated with TAA presented a relatively weak and dark fluorescence signal with an obviously decreased liver area, indicating that TAA exposure could result in the hepatic morphological changes of the larvae. On the contrary, PHI-HA-mEXO treatment dramatically improved the hepatic changes induced by the TAA challenge and dose-dependently enhanced the fluorescence intensity and area. In addition, the zebrafish treated with PHI-HA-mEXO (25, 50, 100 μM) showed a significant improvement in the liver, indicating a superior anti-hepatic fibrosis effect of PHI-HA-mEXO than HA-mEXO, PHI--mEXO, PHI, and mEXO.

3.7. Effect of PHI-HA-mEXO on biochemical indicators

The results of biochemical indicators (ALT, AST, ALP) were shown in Fig. 6B. Compared with the control group, ALT, AST, and ALP levels in the model group were significantly increased, indicating that TAA stimulation could result in liver damage. However, PHI-HA-mEXO (25, 50, 100 μM) treatment significantly reduced ALT, AST, and ALP levels, showing an excellent hepatoprotective effect.

3.8. Effect of PHI-HA-mEXO on histological changes

To further explore the role of PHI-HA-mEXO in liver fibrosis, zebrafish livers were stained with H&E and Sirius red. The results of H&E staining were shown in Fig. 6C. The liver in the control group showed visible nucleoli, round nuclei, and scattered chromatin in the periphery, without cell loss and structural changes. Compared with the control group, the model group showed obvious cell loss and structural changes. However, PHI-HA-mEXO restored liver injury in a dose-dependent manner. Consistent with the changes of H&E staining, the collagen deposition in the model group was significantly increased compared with that in the control group (Fig. 6D). However, PHI-HA-mEXO (25, 50, 100 μM) treatment alleviated collagen deposition in a dose-dependent manner.

3.9. PHI-HA-mEXO inhibited Col1α1 and α-SMA expressions

Col1α1 and α-SMA are important components of extracellular matrix, and their expression levels can reflect the severity of liver fibrosis.

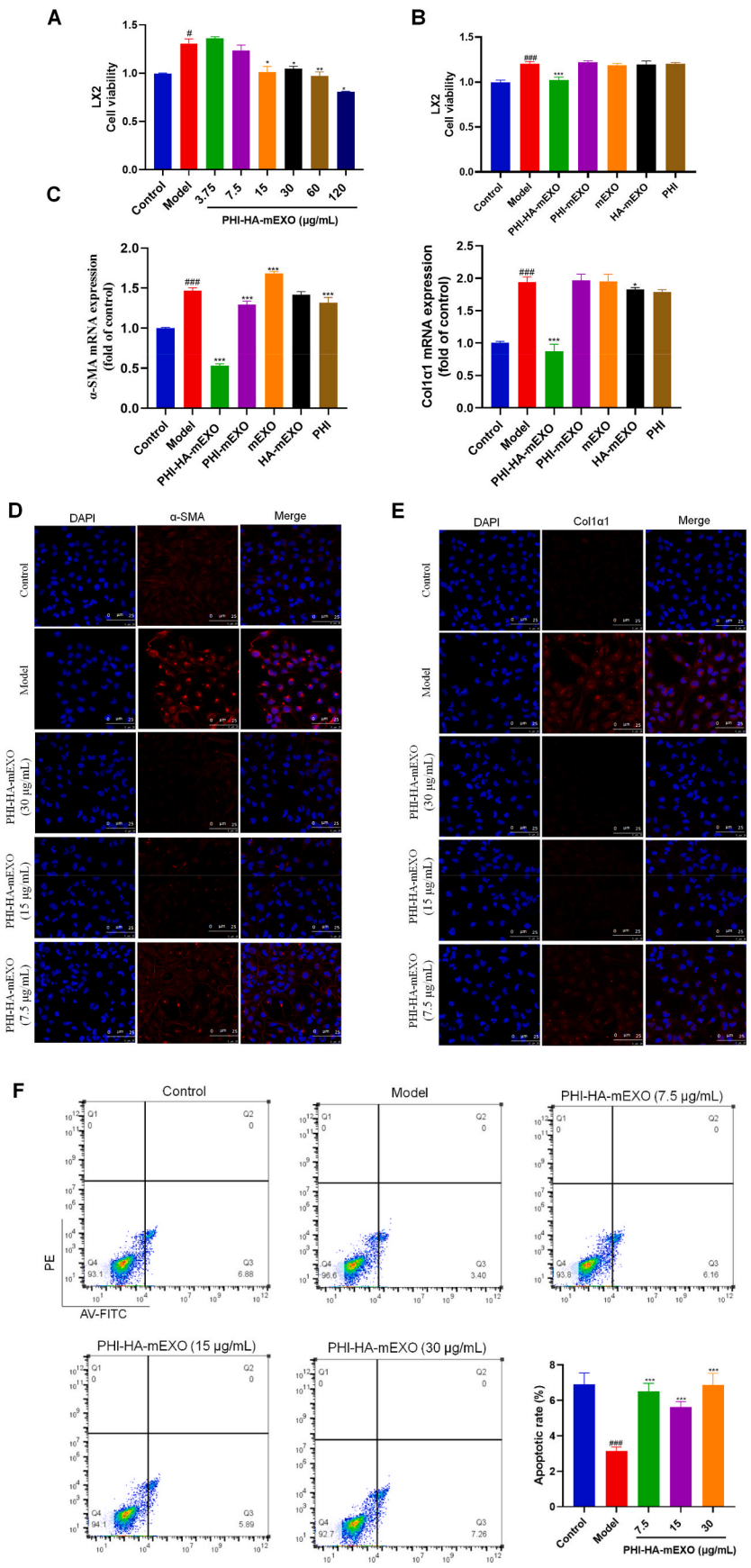

Fig. 4. Anti-hepatic fibrosis effect of PHI-HA-mEXO in vitro. (A) The cell viability of LX2 cells after TGF-β1 and PHI-HA-mEXO (3.75, 7.5, 15, 30, 60 and 120 μg/mL) treatments. (B) Comparison of anti-proliferation effects of mEXO, HA-mEXO, PHI, PHI- mEXO, and PHI-HA-mEXO on TGF-β1-stimulated LX2 cells (n = 6). (C) PHI-HA-mEXO significantly down-regulated α-SMA and Col1α1 mRNA level. (D) Representative images of α-SMA immunofluorescence staining in LX2 cells. (E) Representative images of Col1α1 immunofluorescence staining in LX2 cells. (F) Flow cytometry analysis of LX2 cell apoptosis rate. Each bar represents the mean ± SD (n = 3). $^{\#}p < 0.05$, $^{\#\#}p < 0.01$ and $^{\#\#\#}p < 0.001$ compared with the control group; $^{*}p < 0.05$, $^{**}p < 0.01$ and $^{***}p < 0.001$ compared with the model group.

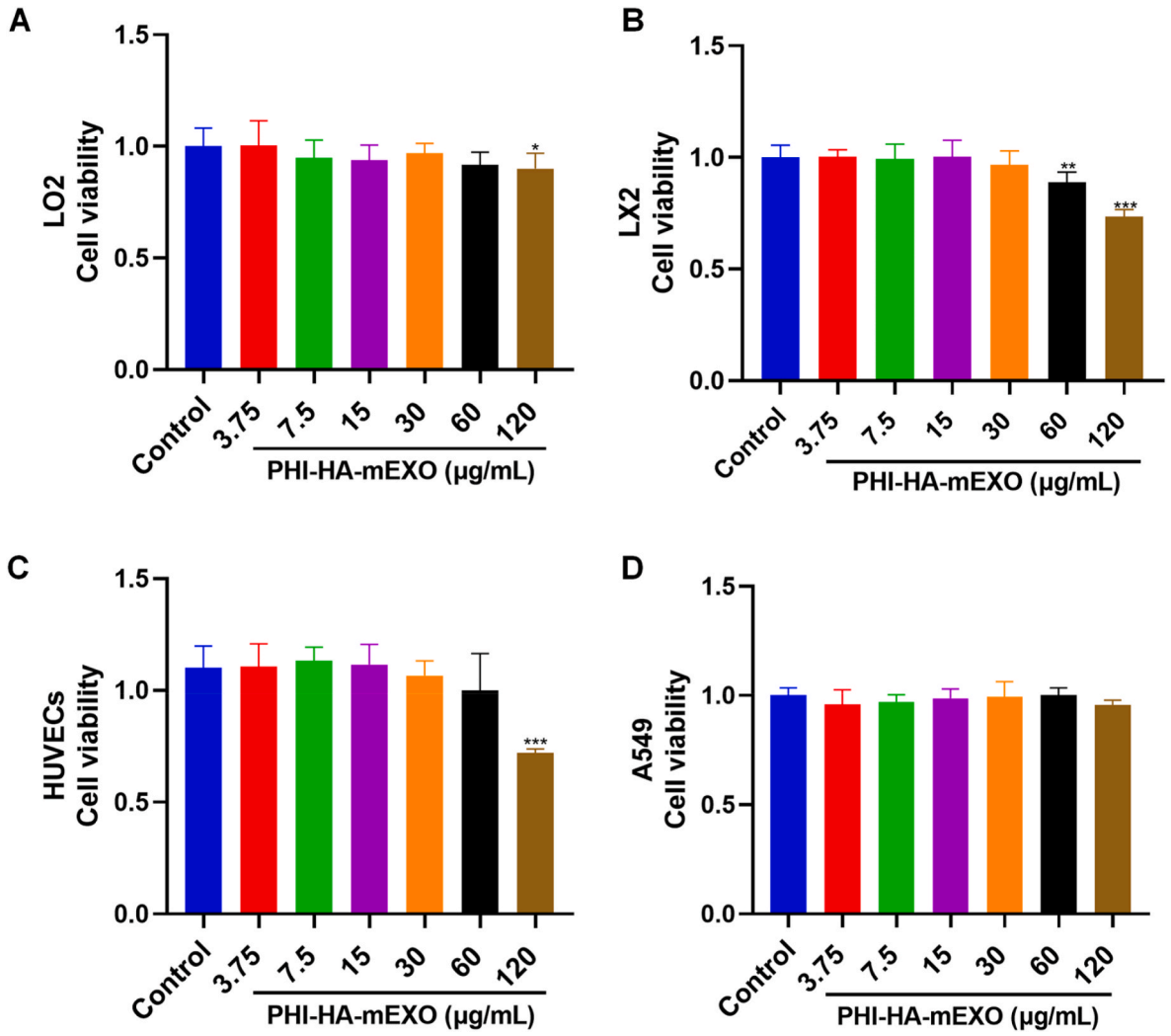

Fig. 5. Effects of PHI-HA-mEXO (3.75, 7.5, 15, 30, 60 and 120 μg/mL) on cells viability. (A) LO2 cells viability. (B) LX2 cells viability. (C) HUVECs cells viability. (D) A549 cells viability. Each bar represents the mean ± SD (n = 6). $^{*}p < 0.05$, $^{**}p < 0.01$ and $^{***}p < 0.001$ compared with the control group.

Therefore, we have carried out RT-qPCR analysis to detect the gene expression changes of Col1α1 and α-SMA in zebrafish (Fig. 6E). The results showed that the expression levels of Col1α1 and α-SMA were significantly increased in the model group, while PHI-HA-mEXO inhibited this change in a dose-dependent manner. The above data clearly showed that PHI-HA-mEXO treatment significantly alleviated TAA-induced liver fibrosis in zebrafish.

3.10. PHI-HA-mEXO inhibited autophagy by activating the PI3K/Akt/mTOR signaling pathway

Autophagy, as a pivotal intracellular pathway, plays a significant role in HSCs activation. Damaged organelles and proteins can be degraded through autophagy to provide energy for activated HSCs to maintain homeostasis [40,41]. Previous studies have confirmed that the PI3K/AKT/mTOR signaling pathway exhibited an important role in HSCs autophagy [42,43]. In order to clarify whether PHI-HA-mEXO inhibits autophagy in aHSCs through the activation of PI3K/Akt/mTOR pathway, mRNA expressions of PI3K, AKT and mTOR were measured. As shown in Fig. 7A, PHI-HA-mEXO treatment significantly increased PI3K, AKT, and mTOR mRNA levels in zebrafish. Therefore, we concluded that the PI3K/Akt/mTOR pathway may be partially involved in PHI-HA-mEXO induced autophagy inhibition of HSCs.

Autophagy can exacerbate liver fibrosis by degrading lipid droplets and cellular proteins to provide energy for aHSCs. Beclin1, LC3 and P62 are the most important markers of autophagosome formation during autophagy. Zebrafish and human have 87% gene homology and similar signaling transduction. Therefore, we conducted RT-qPCR experiments to measure the level of autophagy after PHI-HA-mEXO treatment. The results showed that the expression levels of genes such as Beclin1 and LC3 were significantly increased in the model group (Fig. 7B). However, PHI-HA-mEXO group (25, 50, 100 μM) treatment dose-dependently decreased the levels of Beclin1 and LC3. P62, an autophagy-related transporter, was significantly reduced in the model group and increased in a dose-dependent manner after PHI-HA-mEXO treatment (Fig. 7C). To further confirm our findings, we also analyzed the levels of Atg5 and Atg7 involved in the conversion of LC3-I to LC3-II. As a result, PHI-HA-mEXO significantly reduced the mRNA levels of Atg5 and Atg7 (Fig. 7D). The above results suggested that PHI-HA-mEXO could alleviate liver fibrosis partly by inhibiting autophagy in aHSCs.

4. Discussion

PHI has significant anti-inflammatory and anti-fibrotic effects. However, the poor water solubility and incomplete oral absorption lead to its low oral bioavailability. To overcome the limitations associated with oral administration, a variety of drug delivery systems have been developed. For example, Wang et al. developed a novel self-

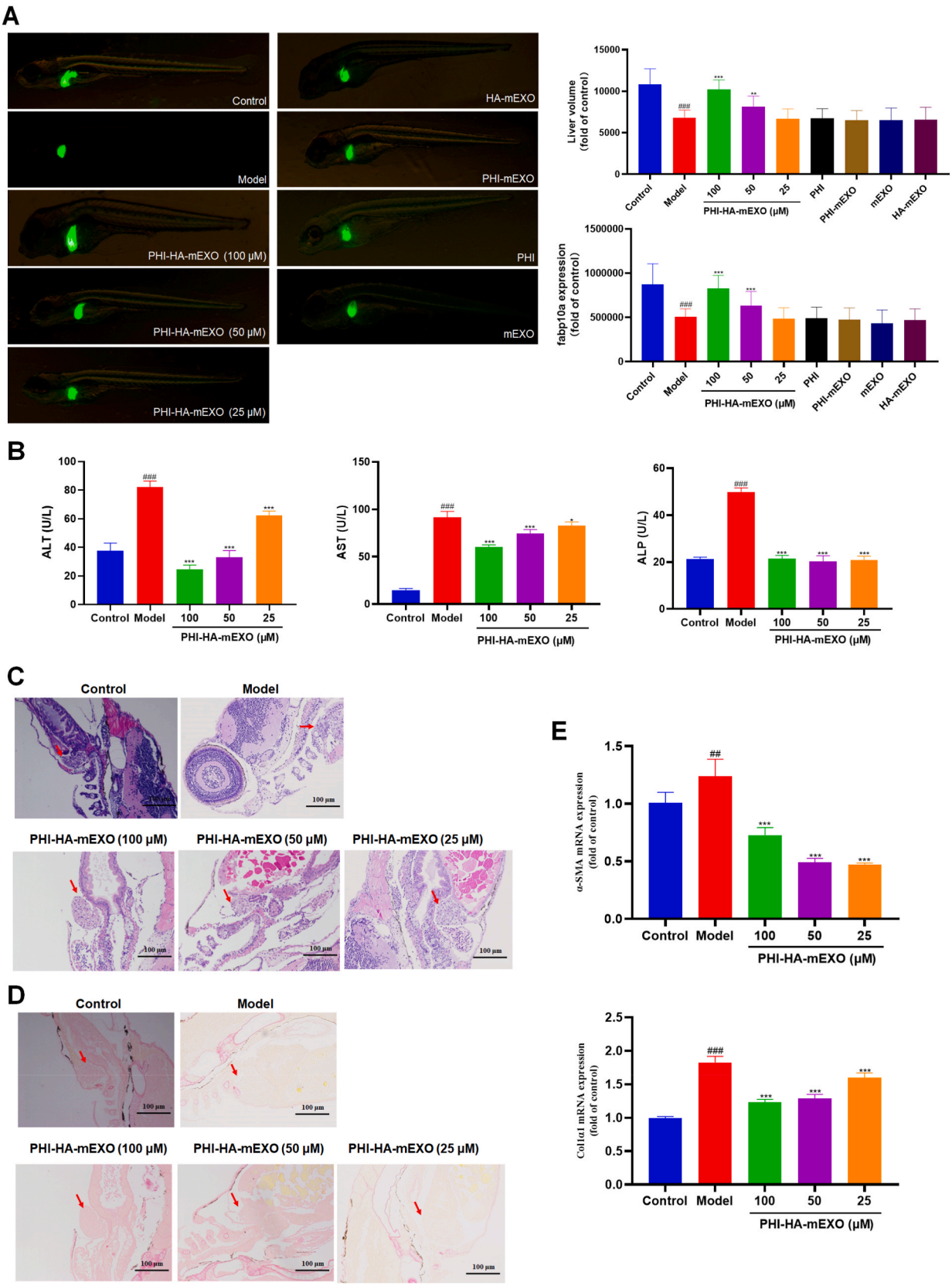

Fig. 6. Anti-liver fibrosis effect of PHI-HA-mEXO in zebrafish model. (A) Representative fluorescence images of zebrafish exposed to TAA, TAA + PHI-HA-mEXO (25, 50, 100 μM), TAA + HA-mEXO, TAA + PHI-mEXO, TAA + PHI, and TAA + mEXO. (B) Effects of PHI-HA-mEXO on ALT, AST and ALP levels in zebrafish larvae. (C) HE staining of the zebrafish liver. (× 200) (D) Sirius red staining of the zebrafish liver. (× 200) (E) Quantitative results of Col1α1 and α-SMA expression in zebrafish. Each bar represents the mean ± SD. $^{\#}p < 0.05$, $^{\#\#}p < 0.01$ and $^{\#\#\#}p < 0.001$ compared with the control group; $^{*}p < 0.05$, $^{**}p < 0.01$ and $^{***}p < 0.001$ compared with the model group. (For interpretation of the references to color in this figure legend, the reader is referred to the Web version of this article.)

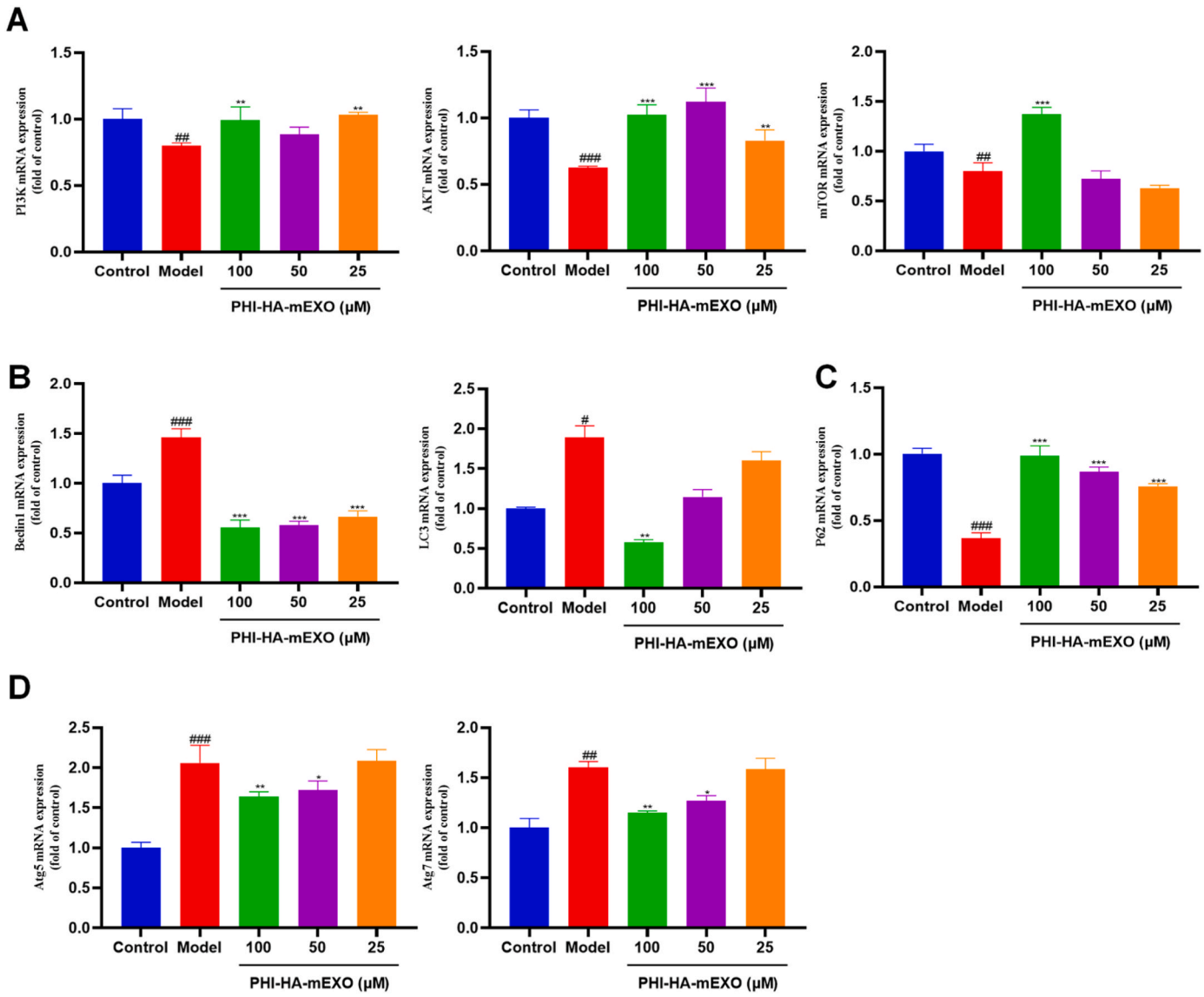

Fig. 7. Effects of PHI-HA-mEXO on autophagy in TAA-induced liver fibrosis in zebrafish. (A) PHI-HA-mEXO effectively changed the mRNA expressions of PI3K, Akt and mTOR. (B) The mRNA expressions of Beclin1 and LC3. (C) The mRNA expression of P62. (D) The mRNA expressions of Atg5 and Atg7. Each bar represents the mean ± SD (n = 3). $^{\#}p < 0.05$, $^{\#\#}p < 0.01$ and $^{\#\#\#}p < 0.001$ compared with the control group; $^{*}p < 0.05$, $^{**}p < 0.01$ and $^{***}p < 0.001$ compared with the model group.

microemulsifying drug delivery system for PHI [44]. However, the high cost, lack of broad applicability, and inherent limitations such as safety greatly limit its clinical application [44]. Our study aimed to develop the oral targeted delivery system for PHI using milk-derived exosomes to improve the bioavailability of PHI and achieve the purpose of targeted therapy. Firstly, milk exosomes were obtained by low-speed centrifugation and high-speed centrifugation in sequence using differential ultracentrifugation. Drug loading was carried out by incubating HA-modified mEXO and PHI at a mass ratio of 6:1 at room temperature for 3 h in the dark. Uncombined PHI was removed by ultrafiltration with a 10 KDa ultrafiltration tube at 3500×*g* for 10 min to obtain the purified PHI-HA-mEXO. Compared with free exosomes (115.9 nm), the morphological size of PHI-HA-mEXO (116 nm) did not change significantly. The interactions between nanoparticles and cell membranes were clearly affected by the surface charge of the nanocomposites. Furthermore, positively charged nanoparticles are more able to induce cellular oxidative stress and disrupt the antioxidant system of hepatocytes. The exosomes showed obvious negative charge, which ensured the safety of the drug delivery system [45].

The stability of extracellular vesicle preparations was crucial in the drug delivery system. The results of the stability experiments showed that the particle size and zeta potential values of PHI-HA-mEXO had no significant change after being stored at −80 °C for one month, indicating a potential storage stability of PHI-HA-mEXO system. In vitro release is another important indicator that can be used to predict the in vivo pharmacokinetics after drug administration. The results of in vitro drug release experiments showed that PHI-HA-mEXO released 46% of the loaded drug within 2 h and 83% within 8 h, indicating a high efficiency of the PHI-HA-mEXO drug delivery system.

As a unique receptor of HA, CD44 is highly expressed in aHSCs during liver fibrosis. Therefore, we used HA to modify mEXO to specifically deliver agents to CD44-overexpressed cells. Our cellular uptake experiments showed that aHSCs exhibited higher uptake compared to qHSCs, suggesting that a large number of CD44 receptors on aHSCs contribute to the enrichment of PHI-HA-mEXO in the disse lumen where HSCs are located in the liver. In addition, DIR-labeled PHI-HA-mEXO showed an increased accumulation in the liver than that of PHI-mEXO, suggesting an improved liver-targeting property of exosomes after HA

decoration.

The cytotoxicity of PHI-HA-mEXO is important for preventing affecting normal HSCs, hepatocytes and other cells during anti-fibrotic therapy. Our cytotoxicity experiments showed that the cell survival rates of normal hepatocytes L02 cells ($CD44^-$), LX2 cells ($CD44^-$), endothelial cells HUVECs ($CD44^+$), and epithelial cells A549 ($CD44^+$) were not affected when the dose of PHI-HA-mEXO was less than 30 μg/mL, but showed an inhibitory effect at a high concentration, suggesting a potential safety of PHI-HA-mEXO in the treatment of liver fibrosis. The in vitro antiproliferative efficacy of PHI-HA-mEXO was tested on aHSCs and the results showed that PHI-HA-mEXO exhibited a superior anti-proliferative effect than free PHI and PHI-mEXO.

Subsequently, we explored the efficacy of PHI-HA-mEXO using a TAA-induced liver fibrosis model in zebrafish. Zebrafish is an ideal model for studying liver disease due to its unique advantages, such as high fecundity, easy breeding, real-time in vivo operation, and the availability of liver-specific transgenic lines [46]. In addition, zebrafish and human have 87% gene homology and shows a 70% similarity to human liver physiology [47–50]. This makes zebrafish an attractive model for liver fibrosis. As a result, PHI-HA-mEXO (25, 50, 100 μM) showed a significant improvement on the damaged liver of zebrafish. In addition, PHI-HA-mEXO treatment significantly reversed the abnormal changes of biochemical indexes ALT, AST and ALP in zebrafish larvae. Compared with the control group, the ALT, AST and ALP levels in zebrafish larvae were significantly increased in the model group, indicating considerable liver function damage in zebrafish. However, after PHI-HA-mEXO treatments, ALT, AST and ALP indexes were significantly reduced, suggesting an excellent anti-fibrotic effect. Furthermore, compared with the model group, the histopathological changes of the liver in the PHI-HA-mEXO group showed decreased collagen fiber formation and focal necrosis in a dose-dependent manner. In conclusion, PHI-HA-mEXO could inhibit HSC activation and reduce col1α1 and α-SMA formation to prevent liver fibrosis.

The activation of HSCs is a typical feature of liver fibrosis. Autophagy, as a highly conserved intracellular degradation pathway, mainly degrades damaged organelles and macromolecules by regulating lysosomes through autophagy-related genes [40]. It has been found that autophagy can provide energy for HSC activation by degrading lipid droplets, and inhibiting autophagy can significantly inhibit HSC activation. Our findings indicated that PHI-HA-mEXO could reverse autophagy-related gene expression including LC3, Beclin1, P62, Atg5 and Atg7 in HSCs. These findings suggested that PHI-HA-mEXO could partially inhibit HSC activation by downregulating autophagy.

In summary, this study suggested that PHI-loaded exosomes showed an enhanced bioavailability and anti-liver fibrosis efficacy following oral administration. As illustrated in Fig. 8, we have successfully developed the nanocarrier of HA-modified milk-derived exosomes encapsulated with PHI for hepatic fibrosis treatment. It was found that HA modification can form a specific ligand-receptor interaction with CD44, and deliver drug-loaded mEXO to the target cells that express CD44 receptors, thus improving the anti-liver fibrosis effect of PHI. However, the detailed pharmacokinetics and dose-response experiments of PHI-HA-mEXO in rodents have not been performed in this study to evaluate the overall effect of oral PHI-HA-mEXO. In addition, further research should be carried out to explore the loading mechanism of exosomes to control the drug loading when applying PHI-HA-mEXO clinically.

5. Conclusion

In this study, we have developed a nanocarrier of HA-modified milk exosomes encapsulated with a natural hepatoprotectant PHI (PHI-HA-mEXO). Our findings indicated that PHI-HA-mEXO could inhibit TGF-β1-stimulated HSC activation and attenuate TAA-induced liver fibrosis in zebrafish. The PHI-HA-mEXO drug delivery system significantly induced apoptosis of aHSCs without affecting normal HSCs and hepatocytes. In addition, PHI-HA-mEXO showed a superior therapeutic effect compared with the same dose of free PHI. The favorable biosafety and significant anti-hepatic fibrosis effect indicated that PHI-HA-mEXO has great potential in the treatment of liver fibrosis. However, the detailed pharmokinetics and dose-responsive experiments of PHI-HA-mEXO and further research on the mechanism of drug loading are still required before PHI-HA-mEXO can be applied clinically.

Author contributions

Lihong Gong: Conducted the experiments, Writing-Original draft preparation, Data curation, Revision. Honglin Zhou: Conceptualization, Review methodology, Conducted the experiments, Writing-Original draft preparation. Cheng Wang and Cheng Ma: Writing-Reviewing and Editing. Yafang Zhang and Ke Fu: Data curation. Yunxia Li: Supervision, Visualization. All the authors read and approved the submitted

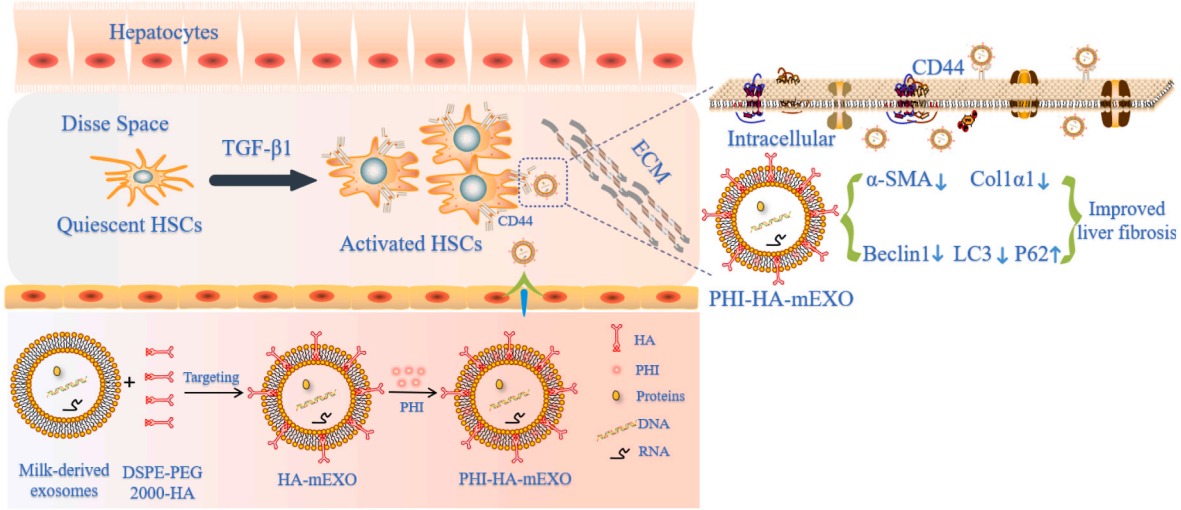

Fig. 8. Schematic representation of CD44 targeting drug delivery system of mEXO loading PHI for treatment of liver fibrosis. Using engineered mEXO that specifically targeting CD44, hepatoprotective agents PHI can be efficiently delivered to the activated hepatic stellate cells and inhibit their activation. The engineered mEXO showed hepatoprotective activities in the treatment of liver fibrosis both in vivo and in vitro, suggesting a target drug delivery therapy based on engineered mEXO for alleviating liver fibrosis. The upward arrow represents the promotion of PHI-HA-mEXO, and the downward arrow represents the inhibition of PHI-HA-mEXO.

manuscript.

Declarations

Ethics approval and consent to participate. The Ethical Committee of Chengdu University of Traditional Chinese Medicine approved all animal experiments.

Consent for publication

All the co-authors were aware of this submission and approve for publication.

Funding

The work was supported by National Natural Science Foundation of China (No: 81891012, U19A2010, 81630101), Innovation Team and Talents Cultivation Program of National Administration of Traditional Chinese Medicine (No: ZYYCXTD-D-202209), Sichuan Province Science and Technology Support Program (No: 2021JDRC0041, 2022ZYD0088) and Sichuan TCM Science and Technology Industry Innovation Team (NO: 2022C001).

Declaration of competing interest

The authors declare that they have no known competing financial interests or personal relationships that could have appeared to influence the work reported in this paper.

Data availability

Data will be made available on request.

Abbreviations

PHI	Phillygenin
Phillygenin-HA composite exosomes	PHI-HA-mEXO
mEXO	Milk-derived exosomes
HA	hyaluronic acid
aHSCs	activated hepatic stellate cells
qHSCs	quiescent hepatic stellate cells
TAA	thioacetamide
HPLC	high performance liquid chromatography

Appendix A. Supplementary data

Supplementary data to this article can be found online at https://doi.org/10.1016/j.mtbio.2023.100804.

References

[1] T. Kisseleva, D.J.N.r.G. Brenner, hepatology, Molecular and cellular mechanisms of liver fibrosis and its regression 18 (2021) 151–166, https://doi.org/10.1038/s41575-020-00372-7.

[2] J. Berumen, J. Baglieri, T. Kisseleva, K.J.W.m.o.d. Mekeel, Liver fibrosis: Pathophysiology and clinical implications 13 (2021) e1499, https://doi.org/10.1002/wsbm.1499.

[3] S. Kumar, Q. Duan, R. Wu, E. Harris, Q.J.A.d.d.r. Su, Pathophysiological communication between hepatocytes and non-parenchymal cells in liver injury from, NAFLD to liver fibrosis 176 (2021), 113869, https://doi.org/10.1016/j.addr.2021.113869.

[4] D. Cheng, J. Chai, H. Wang, L. Fu, S. Peng, X.J.L.i.o.j.o.t.I.A.f.t.S.o.t.L. Ni, Hepatic macrophages, Key players in the development and progression of liver fibrosis 41 (2021) 2279–2294, https://doi.org/10.1111/liv.14940.

[5] B. Foglia, E. Novo, F. Protopapa, M. Maggiora, C. Bocca, S. Cannito, M.J.C. Parola, Hypoxia, Hypoxia-Inducible Factors and Liver Fibrosis, vol. 10, 2021, https://doi.org/10.3390/cells10071764.

[6] M. Virarkar, A. Morani, M. Taggart, P.J.S.i.u. Bhosale, M.R. Ct, Liver Fibrosis Assessment 42 (2021) 381–389, https://doi.org/10.1053/j.sult.2021.03.003.

[7] A. Caligiuri, A. Gentilini, M. Pastore, S. Gitto, F.J.C. Marra, Cellular and Molecular Mechanisms Underlying Liver Fibrosis Regression, vol. 10, 2021, https://doi.org/10.3390/cells10102759.

[8] A. Altamirano-Barrera, B. Barranco-Fragoso, N.J.A.o.h. Méndez-Sánchez, Management strategies for liver fibrosis 16 (2017) 48–56, https://doi.org/10.5604/16652681.1226814.

[9] Y. Liu, S. Qi, K.J.A.o.p.m. Sun, Traditional Chinese medicine, liver fibrosis, intestinal flora: is there any connection? -a narrative review 10 (2021) 4846–4857, https://doi.org/10.21037/apm-20-2129.

[10] N. Hu, C. Wang, X. Dai, M. Zhou, L. Gong, L. Yu, C. Peng, Y.J.J.o.e. Li, Phillygenin inhibits LPS-induced activation and inflammation of LX2 cells by TLR4/MyD88/NF-κB signaling pathway 248 (2020), 112361, https://doi.org/10.1016/j.jep.2019.112361.

[11] C. Wang, C. Ma, K. Fu, L. Gong, Y. Zhang, H. Zhou, Y.J.F.i.p. Li, viaPhillygenin attenuates carbon tetrachloride-induced liver fibrosis, Modulating Inflammation and Gut Microbiota 12 (2021), 756924, https://doi.org/10.3389/fphar.2021.756924.

[12] C. Wang, C. Ma, K. Fu, Y. Liu, L. Gong, C. Peng, Y.J.J.o.e. Li, Hepatoprotective effect of phillygenin on carbon tetrachloride-induced liver fibrosis and its effects on short chain, fatty acid and bile acid metabolism 296 (2022), 115478, https://doi.org/10.1016/j.jep.2022.115478.

[13] W. Song, J. Wu, L. Yu, Z.J.B.r.i. Peng, Evaluation of the Pharmacokinetics and Hepatoprotective Effects of Phillygenin in Mouse, 2018, 2018, 7964318, https://doi.org/10.1155/2018/7964318.

[14] L. Wang, W. Yan, Y. Tian, H. Xue, J. Tang, L.J.P. Zhang, Self-microemulsifying drug delivery system of phillygenin: formulation development, Characterization and Pharmacokinetic Evaluation 12 (2020), https://doi.org/10.3390/pharmaceutics12020130.

[15] E. Batrakova, M.J.J.o.c.r.o.j.o.t.C.R.S. Kim, Using exosomes, naturally-equipped nanocarriers, Drug Deliv. 219 (2015) 396–405, https://doi.org/10.1016/j.jconrel.2015.07.030.

[16] W. Meng, C. He, Y. Hao, L. Wang, L. Li, G.J.D.d. Zhu, Prospects and challenges of extracellular vesicle-based drug delivery system, considering cell source 27 (2020) 585–598, https://doi.org/10.1080/10717544.2020.1748758.

[17] R. Munagala, F. Aqil, J. Jeyabalan, R. Gupta, Bovine milk-derived exosomes for drug delivery, Cancer Lett. 371 (2016) 48–61, https://doi.org/10.1016/j.canlet.2015.10.020.

[18] S. Li, Y. Tang, Y.J.C.d.d. Dou, The Potential of Milk-Derived Exosomes for Drug Delivery 18 (2021) 688–699, https://doi.org/10.2174/1567201817666200817112503.

[19] L. Wu, L. Wang, X. Liu, Y. Bai, R. Wu, X. Li, Y. Mao, L. Zhang, Y. Zheng, T. Gong, Z. Zhang, Y.J.A.p.S.B. Huang, Milk-derived exosomes exhibit versatile effects for improved oral drug delivery 12 (2022) 2029–2042, https://doi.org/10.1016/j.apsb.2021.12.015.

[20] N. Roehlen, E. Crouchet, T.J.C. Baumert, Liver Fibrosis: Mechanistic Concepts and Therapeutic Perspectives, vol. 9, 2020, https://doi.org/10.3390/cells9040875.

[21] K. Choi, H. Han, E. Lee, J. Shin, B. Almquist, D. Lee, J.J.A.m. Park, Hyaluronic acid-based activatable nanomaterials for stimuli-responsive imaging and therapeutics: beyond CD44-mediated, Drug Deliv. 31 (2019), e1803549, https://doi.org/10.1002/adma.201803549.

[22] W. Li, C. Zhou, Y. Fu, T. Chen, X. Liu, Z. Zhang, T.J.A.p.S.B. Gong, Targeted delivery of hyaluronic acid nanomicelles to hepatic stellate cells in hepatic fibrosis rats 10 (2020) 693–710, https://doi.org/10.1016/j.apsb.2019.07.003.

[23] N. Zarovni, A. Corrado, P. Guazzi, D. Zocco, E. Lari, G. Radano, J. Muhhina, C. Fondelli, J. Gavrilova, A. Chiesi, Integrated isolation and quantitative analysis of exosome shuttled proteins and nucleic acids using immunocapture approaches, Methods 87 (2015) 46–58, https://doi.org/10.1016/j.ymeth.2015.05.028.

[24] L. Muller, C.S. Hong, D.B. Stolz, S.C. Watkins, T.L. Whiteside, Isolation of biologically-active exosomes from human plasma, J. Immunol. Methods 411 (2014) 55–65, https://doi.org/10.1016/j.jim.2014.06.007.

[25] T.F. Hiemstra, P.D. Charles, T. Gracia, S.S. Hester, L. Gatto, R. Al-Lamki, R.A. Floto, Y. Su, J.N. Skepper, K.S. Lilley, F.E. Karet Frankl, Human urinary exosomes as innate immune effectors, J. Am. Soc. Nephrol. 25 (2014) 2017–2027, https://doi.org/10.1681/asn.2013101066.

[26] L.M. Doyle, M.Z. Wang, Overview of extracellular vesicles, their origin, composition, purpose, and methods for exosome isolation and analysis, Cells 8 (2019), https://doi.org/10.3390/cells8070727.

[27] R. Szatanek, J. Baran, M. Siedlar, M. Baj-Krzyworzeka, Isolation of extracellular vesicles: determining the correct approach (Review), Int. J. Mol. Med. 36 (2015) 11–17, https://doi.org/10.3892/ijmm.2015.2194.

[28] H. Izumi, M. Tsuda, Y. Sato, N. Kosaka, T. Ochiya, H. Iwamoto, K. Namba, Y. Takeda, Bovine milk exosomes contain microRNA and mRNA and are taken up by human macrophages, J. Dairy Sci. 98 (2015) 2920–2933, https://doi.org/10.3168/jds.2014-9076.

[29] D. Li, S. Yao, Z. Zhou, J. Shi, Z. Huang, Z. Wu, Hyaluronan decoration of milk exosomes directs tumor-specific delivery of doxorubicin, Carbohydr. Res. 493 (2020), 108032, https://doi.org/10.1016/j.carres.2020.108032.

[30] L. Gong, H. He, D. Li, L. Cao, T.A. Khan, Y. Li, L. Pan, L. Yan, X. Ding, Y. Sun, Y. Zhang, G. Yi, S. Hu, L. Xia, A new isolate of pediococcus pentosaceus (SL001) with antibacterial activity against fish pathogens and potency in facilitating the immunity and growth performance of grass carps, Front. Microbiol. 10 (2019) 1384, https://doi.org/10.3389/fmicb.2019.01384.

[31] J. Zhang, Y. Deng, B. Cheng, Y. Huang, Y. Meng, K. Zhong, G. Xiong, J. Guo, Y. Liu, H. Lu, Protective effects and molecular mechanisms of baicalein on thioacetamide-induced toxicity in zebrafish larvae, Chemosphere 256 (2020), 127038, https://doi.org/10.1016/j.chemosphere.2020.127038.

[32] H. Izumi, N. Kosaka, T. Shimizu, K. Sekine, T. Ochiya, M. Takase, Bovine milk contains microRNA and messenger RNA that are stable under degradative conditions, J. Dairy Sci. 95 (2012) 4831–4841, https://doi.org/10.3168/jds.2012-5489.
[33] I. Van Hese, K. Goossens, L. Vandaele, G. Opsomer, Invited review: MicroRNAs in bovine colostrum-Focus on their origin and potential health benefits for the calf, J. Dairy Sci. 103 (2020) 1–15, https://doi.org/10.3168/jds.2019-16959.
[34] S. Shandilya, P. Rani, S.K. Onteru, D. Singh, Small interfering RNA in milk exosomes is resistant to digestion and crosses the intestinal barrier in vitro, J. Agric. Food Chem. 65 (2017) 9506–9513, https://doi.org/10.1021/acs.jafc.7b03123.
[35] M. Vashisht, P. Rani, S.K. Onteru, D. Singh, Curcumin encapsulated in milk exosomes resists human digestion and possesses enhanced intestinal permeability in vitro, Appl. Biochem. Biotechnol. 183 (2017) 993–1007, https://doi.org/10.1007/s12010-017-2478-4.
[36] M.S. Lord, B.L. Farrugia, C.M. Yan, J.A. Vassie, J.M. Whitelock, Hyaluronan coated cerium oxide nanoparticles modulate CD44 and reactive oxygen species expression in human fibroblasts, J. Biomed. Mater. Res. 104 (2016) 1736–1746, https://doi.org/10.1002/jbm.a.35704.
[37] J.P. Iredale, R.C. Benyon, J. Pickering, M. McCullen, M. Northrop, S. Pawley, C. Hovell, M.J. Arthur, Mechanisms of spontaneous resolution of rat liver fibrosis. Hepatic stellate cell apoptosis and reduced hepatic expression of metalloproteinase inhibitors, J. Clin. Invest. 102 (1998) 538–549, https://doi.org/10.1172/jci1018.
[38] B. Saile, T. Knittel, N. Matthes, P. Schott, G. Ramadori, CD95/CD95L-mediated apoptosis of the hepatic stellate cell. A mechanism terminating uncontrolled hepatic stellate cell proliferation during hepatic tissue repair, Am. J. Pathol. 151 (1997) 1265–1272.
[39] D. van der Helm, A. Groenewoud, E.S.M. de Jonge-Muller, M.C. Barnhoorn, M.J. A. Schoonderwoerd, M.J. Coenraad, L. Hawinkels, B.E. Snaar-Jagalska, B. van Hoek, H.W. Verspaget, Mesenchymal stromal cells prevent progression of liver fibrosis in a novel zebrafish embryo model, Sci. Rep. 8 (2018), 16005, https://doi.org/10.1038/s41598-018-34351-5.
[40] A. Mallat, J. Lodder, F. Teixeira-Clerc, R. Moreau, P. Codogno, S. Lotersztajn, Autophagy: a multifaceted partner in liver fibrosis, BioMed Res. Int. 2014 (2014), 869390, https://doi.org/10.1155/2014/869390.
[41] A.Y. Xiu, Q. Ding, Z. Li, C.Q. Zhang, Doxazosin attenuates liver fibrosis by inhibiting autophagy in hepatic stellate cells via activation of the PI3K/Akt/mTOR signaling pathway, Drug Des Devel Ther 15 (2021) 3643–3659, https://doi.org/10.2147/dddt.s317701.
[42] L. Ba, J. Gao, Y. Chen, H. Qi, C. Dong, H. Pan, Q. Zhang, P. Shi, C. Song, X. Guan, Y. Cao, H. Sun, Allicin attenuates pathological cardiac hypertrophy by inhibiting autophagy via activation of PI3K/Akt/mTOR and MAPK/ERK/mTOR signaling pathways, Phytomedicine 58 (2019), 152765, https://doi.org/10.1016/j.phymed.2018.11.025.
[43] P. Varshney, N. Saini, PI3K/AKT/mTOR activation and autophagy inhibition plays a key role in increased cholesterol during IL-17A mediated inflammatory response in psoriasis, Biochim. Biophys. Acta, Mol. Basis Dis. 1864 (2018) 1795–1803, https://doi.org/10.1016/j.bbadis.2018.02.003.
[44] L. Wang, W. Yan, Y. Tian, H. Xue, J. Tang, L. Zhang, Self-microemulsifying drug delivery system of phillygenin: formulation development, characterization and pharmacokinetic evaluation, Pharmaceutics 12 (2020), https://doi.org/10.3390/pharmaceutics12020130.
[45] G. Midekessa, K. Godakumara, J. Ord, J. Viil, F. Lättekivi, K. Dissanayake, S. Kopanchuk, A. Rinken, A. Andronowska, S. Bhattacharjee, T. Rinken, A. Fazeli, Zeta potential of extracellular vesicles: toward understanding the attributes that determine colloidal stability, ACS Omega 5 (2020) 16701–16710, https://doi.org/10.1021/acsomega.0c01582.
[46] K. Dooley, L.I. Zon, Zebrafish: a model system for the study of human disease, Curr. Opin. Genet. Dev. 10 (2000) 252–256, https://doi.org/10.1016/s0959-437x(00)00074-5.
[47] W. Goessling, K.C. Sadler, Zebrafish, An important tool for liver disease research, Gastroenterology 149 (2015) 1361–1377, https://doi.org/10.1053/j.gastro.2015.08.034.
[48] G.J. Lieschke, P.D. Currie, Animal models of human disease: zebrafish swim into view, Nat. Rev. Genet. 8 (2007) 353–367, https://doi.org/10.1038/nrg2091.
[49] C. Yin, K.J. Evason, J.J. Maher, D.Y. Stainier, The basic helix-loop-helix transcription factor, heart and neural crest derivatives expressed transcript 2, marks hepatic stellate cells in zebrafish: analysis of stellate cell entry into the developing liver, Hepatology 56 (2012) 1958–1970, https://doi.org/10.1002/hep.25757.
[50] K. Howe, M.D. Clark, C.F. Torroja, J. Torrance, C. Berthelot, M. Muffato, J. E. Collins, S. Humphray, K. McLaren, L. Matthews, S. McLaren, I. Sealy, M. Caccamo, C. Churcher, C. Scott, J.C. Barrett, R. Koch, G.J. Rauch, S. White, W. Chow, B. Kilian, L.T. Quintais, J.A. Guerra-Assunção, Y. Zhou, Y. Gu, J. Yen, J. H. Vogel, T. Eyre, S. Redmond, R. Banerjee, J. Chi, B. Fu, E. Langley, S.F. Maguire, G.K. Laird, D. Lloyd, E. Kenyon, S. Donaldson, H. Sehra, J. Almeida-King, J. Loveland, S. Trevanion, M. Jones, M. Quail, D. Willey, A. Hunt, J. Burton, S. Sims, K. McLay, B. Plumb, J. Davis, C. Clee, K. Oliver, R. Clark, C. Riddle, D. Elliot, G. Threadgold, G. Harden, D. Ware, S. Begum, B. Mortimore, G. Kerry, P. Heath, B. Phillimore, A. Tracey, N. Corby, M. Dunn, C. Johnson, J. Wood, S. Clark, S. Pelan, G. Griffiths, M. Smith, R. Glithero, P. Howden, N. Barker, C. Lloyd, C. Stevens, J. Harley, K. Holt, G. Panagiotidis, J. Lovell, H. Beasley, C. Henderson, D. Gordon, K. Auger, D. Wright, J. Collins, C. Raisen, L. Dyer, K. Leung, L. Robertson, K. Ambridge, D. Leongamornlert, S. McGuire, R. Gilderthorp, C. Griffiths, D. Manthravadi, S. Nichol, G. Barker, S. Whitehead, M. Kay, J. Brown, C. Murnane, E. Gray, M. Humphries, N. Sycamore, D. Barker, D. Saunders, J. Wallis, A. Babbage, S. Hammond, M. Mashreghi-Mohammadi, L. Barr, S. Martin, P. Wray, A. Ellington, N. Matthews, M. Ellwood, R. Woodmansey, G. Clark, J. Cooper, A. Tromans, D. Grafham, C. Skuce, R. Pandian, R. Andrews, E. Harrison, A. Kimberley, J. Garnett, N. Fosker, R. Hall, P. Garner, D. Kelly, C. Bird, S. Palmer, I. Gehring, A. Berger, C.M. Dooley, Z. Ersan-Ürün, C. Eser, H. Geiger, M. Geisler, L. Karotki, A. Kirn, J. Konantz, M. Konantz, M. Oberländer, S. Rudolph-Geiger, M. Teucke, C. Lanz, G. Raddatz, K. Osoegawa, B. Zhu, A. Rapp, S. Widaa, C. Langford, F. Yang, S.C. Schuster, N.P. Carter, J. Harrow, Z. Ning, J. Herrero, S.M. Searle, A. Enright, R. Geisler, R.H. Plasterk, C. Lee, M. Westerfield, P.J. de Jong, L.I. Zon, J.H. Postlethwait, C. Nüsslein-Volhard, T.J. Hubbard, H. Roest Crollius, J. Rogers, D.L. Stemple, The zebrafish reference genome sequence and its relationship to the human genome, Nature 496 (2013) 498–503, https://doi.org/10.1038/nature12111.